Climate Dynamics (2019) 52:5585–5604
https://doi.org/10.1007/s00382-018-4464-0

Solar impacts on decadal variability of tropopause temperature and lower stratospheric (LS) water vapour: a mechanism through ocean–atmosphere coupling

Wuke Wang[1,2,3] · **Katja Matthes**[4,5] · **Wenshou Tian**[6] · **Wonsun Park**[4] · **Ming Shangguan**[7] · **Aijun Ding**[1,2,3]

Received: 2 January 2018 / Accepted: 21 September 2018 / Published online: 29 September 2018

Abstract

Solar signals in the atmosphere and the ocean, especially in tropopause temperatures and lower stratospheric water vapour are investigated using recent observational and reanalyses data sets for the period from 1958 through 2013. Previous observational and modeling studies demonstrated solar influences in the lower stratosphere resembling a positive Northern Annular Mode due to the top-down mechanism involving enhanced solar UV radiation in the stratosphere during solar maxima and dynamical amplification mechanisms in the atmosphere. We found that these stratospheric changes might propagate down to the troposphere and become zonally asymmetric with characteristic pressure and wind pattern over the North Atlantic and North Pacific. Such changes in tropospheric circulation are related to anomalous positive SST anomalies in the central Pacific which resemble an El Niño Modoki event. We show for the first time with ocean reanalysis data that these SST anomalies are amplified by a positive feedback through oceanic subsurface currents and heat transport in the equatorial Pacific. Anomalous warm SSTs in the equatorial central Pacific change the zonal SST gradient and lead to anomalous westerly winds and currents in the western Pacific and easterly winds and currents in the eastern Pacific. This indicates a convergence and less upwelling and therefore enhances the positive SST anomalies in the equatorial central Pacific. Such a positive feedback results in a peak of El Niño Modoki events about 2 years after the solar maximum. These solar-induced signals in the ocean in turn modify the circulation and convection in the troposphere, resulting in lagged solar signals of anomalous high tropopause heights and negative anomalies in tropopause temperatures as well as in lower stratospheric water vapour over the equatorial Pacific which are in agreement with a time evolving solar-induced El Niño Modoki-like SST pattern. We demonstrate a solar modulation of intrinsic decadal climate variability over the Pacific which is amplified by positive feedbacks between the ocean and the atmosphere.

Keywords 11-Year solar cycle · TropoPause temperature (TPT) · Decadal variability · Lower stratospheric (LS)water vapour · Sea surface temperature (SST)

Electronic supplementary material The online version of this article (https://doi.org/10.1007/s00382-018-4464-0) contains supplementary material, which is available to authorized users.

✉ Wuke Wang
wuke.wang@nju.edu.cn

✉ Katja Matthes
kmatthes@geomar.de

[1] Institute for Climate and Global Change Research, School of Atmospheric Sciences, Nanjing University, Nanjing, China

[2] Joint International Research Laboratory of Atmospheric and Earth System Sciences (JirLATEST), Nanjing University, Nanjing, China

[3] Collaborative Innovation Center of Climate Change, Nanjing, Jiangsu, China

[4] GEOMAR Helmholtz-Zentrum für Ozeanforschung Kiel, Kiel, Germany

[5] Christian-Albrechts-Universität zu Kiel, Kiel, Germany

[6] College of Atmospheric Sciences, Lanzhou University, Lanzhou, China

[7] School of Transportation, Southeast University, Nanjing, China

1 Introduction

The Sun is the energy source of the climate system. The total solar irradiance (TSI) varies with a clear 11 year solar cycle but a small amplitude of about 0.1% (1.3 W m^{-2}) (Kopp and Lean 2011). However, the amplitude of the 11-year solar cycle in the UV band is much larger by about 8% in the wavelength range important for ozone formation and middle atmosphere heating (Lean et al. 1995) and directly affect temperatures in the upper stratosphere (Gray et al. 2010; Mitchell et al. 2015; Kodera et al. 2016). Several amplifying mechanisms have been proposed and suggest that regional responses to the solar cycle in both the upper atmosphere and surface climate are significant (Kodera and Kuroda 2002; Matthes et al. 2006; Meehl et al. 2009; Gray et al. 2010; Scaife et al. 2013; Thiéblemont et al. 2015). One amplification mechanism is the so-called "top-down" mechanism which involves enhanced UV radiation, increased temperatures in the equatorial upper stratosphere and hence a strengthening of the meridional temperature gradient which in turn changes the propagation properties of planetary waves and leads to a poleward–downward transport of the solar signal through dynamical wave-mean flow interactions. The poleward–downward movement of the stratospheric zonal wind jet projects onto the Northern Annular Mode (NAM) in the lower stratosphere and leads to a poleward shift of the jet streams over the North Atlantic and the North Pacific (Matthes et al. 2006; Kodera et al. 2016). At the same time the stratospheric Brewer–Dobson circulation is weakened and results in a secondary temperature maximum in the tropical lower stratosphere (Gray et al. 2010; Mitchell et al. 2015; Kodera et al. 2016). There is still a debate whether this secondary warming is not only related to solar but also to aliasing effects with volcanoes and the El Niño Southern Oscillation (ENSO) (Marsh and Garcia 2007; Gray et al. 2010; Chiodo et al. 2014). Another amplification mechanism is the so-called "bottom-up" mechanism which involves an amplification of the small direct signal at the Earth's and ocean surface, in particular in the equatorial Pacific through atmosphere–ocean coupling (White et al. 1997; Meehl et al. 2009).

In the tropical Pacific, observational evidence for solar signals in SSTs is not clear. Several studies reveal a La Niña-like SST pattern (van Loon and Meehl 2008; Meehl et al. 2009; Gray et al. 2010), while some other studies reported an El Niño-like response (Roy and Haigh 2010) or neither of both (Tung and Zhou 2010; Zhou and Tung 2010). This inconsistency of previous studies results from different analysis methods as well as different time periods (Kodera et al. 2016). For example, Meehl et al. (2009) selected solar peak years from 1850 to 2002, Roy and Haigh (2010) applied a multiple linear regression for the period 1850–2004, while a composite-mean difference (CMD) of 1880–2007 is used in Zhou and Tung (2010). Despite these discrepancies, some common features can be seen during solar maximum years in SSTs over the Pacific: positive SST anomalies occur in the central Pacific and surround the western coast of North America (Tung and Zhou 2010; Gray et al. 2013), and negative anomalies occur over the cold tongue region (van Loon and Meehl 2008; Kodera et al. 2016). Recent studies indicated that SST responses to the solar cycle resemble an El Niño-Modoki (central Pacific El Niño) pattern (Kodera et al. 2016; Huo and Xiao 2017).

The SST response to solar cycle variability is not only associated with relatively fast (a couple of months) processes in the atmosphere, but also involves slow processes related to atmosphere–ocean coupling and oceanic circulations. Therefore, a time lag is expected in a possible solar cycle response of the ocean. A time lag of 2–3 years has been reported in observed SST associated with the 11-year solar cycle over the North Atlantic (Gray et al. 2013), and has been related to a combined mechanism of air–sea interactions and a downward propagation of solar-induced anomalous stratospheric circulation (Scaife et al. 2013; Thiéblemont et al. 2015). A time lag in SSTs has also been noticed over the Pacific (White et al. 1997; Meehl and Arblaster 2009; Misios et al. 2016; Huo and Xiao 2017), with a possible "delayed action oscillator" mechanism (White and Liu 2008). Beside the above described signals at the surface, we expect solar signals also in the ocean. However, because of the lack of oceanic subsurface data, most previous studies of solar influences are limited to the analysis of SSTs. Therefore, solar-induced responses in the ocean have been investigated mostly in model simulations. Recently, oceanic reanalysis data are available (Balmaseda et al. 2013) and provide a new opportunity to detect solar signals in the ocean. One main goal of this work is to detect solar signals in the ocean, using a combined approach of both SST observations and oceanic reanalysis. In particular, time lags will be considered to analyze the signal evolution during the solar cycle in order to better understand the underlying mechanisms.

At the same time, lagged solar signals in the ocean in turn have the potential to force the overlying atmosphere. Currently, such lagged signals in the atmosphere associated with the 11-year solar cycle and subsequent SST anomalies have been less investigated (Misios et al. 2016). The second goal of this research is to analyze exactly these solar signals in the atmosphere associated with lagged solar signals in the ocean. We will in particular focus on lagged solar signals around the tropical tropopause, a region rarely investigated, but very important for global climate.

The tropopause is sensitive to both stratospheric and tropospheric thermal-dynamical changes and is especially important for troposphere–stratosphere coupling. Investigating the solar influences on the tropopause is therefore particularly helpful to unveil the mechanism of the solar impacts on both the troposphere and the stratosphere. Recent results showed that beside the long-term trend (Randel et al. 2006; Rosenlof and Reid 2008; Gettelman et al. 2010; Xie et al. 2014), there are also significant decadal to multi-decadal variabilities in tropical tropopause temperatures (Wang et al. 2012; Fueglistaler et al. 2013; Wang et al. 2013, 2015, 2016). Wang et al. (2016) indicated that, the Pacific Decadal Oscillation (PDO) as well as the 11-year solar cycle are important for a model to simulate the decadal variability of tropical tropopause temperatures. However, a possible mechanism of the later is still missing.

Tropopause temperatures in the tropics determine the amount of water vapour entering the stratosphere, which is an important radiative gas for surface climate (Solomon et al. 2010; Dessler et al. 2013; Gilford et al. 2016; Wang et al. 2017). Analyses from balloon measurements in Boulder show an significant increase of lower stratospheric (LS) water vapour for the period 1980–2010 (Hurst et al. 2011), while other studies do not find a clear long-term trend (Dessler et al. 2014; Hegglin et al. 2014). Several studies noticed that LS water vapour rather has decadal variability (Fueglistaler et al. 2013; Hegglin et al. 2014; Dessler et al. 2014; Schieferdecker et al. 2015; Wang et al. 2016) than any sign of anthropogenic trend in both model and observational studies (Hurst et al. 2011). In particular, a recent study indicated that the solar cycle is leading the LS water vapour by about 2 years in its decadal variability (Schieferdecker et al. 2015). Processes related to the decadal variability in tropopause temperatures and LS water vapour, in particular the role of the solar cycle, the atmosphere and the ocean are open questions which we would like to address in this paper.

In addition, most previous studies used zonal mean data in investigating the variability of tropopause temperatures and LS water vapour. However, the zonal structure of tropopause temperature variations, as reported by several recent studies, is important, since it is helpful to unveil the mechanisms in response to climate changes (Garfinkel et al. 2013a; Fu 2013; Hu et al. 2016). Therefore a special focus will be given here to the zonally asymmetric structure of tropopause temperatures and lower stratospheric water vapour.

In this study, we first investigate the 11-year solar cycle related signals in SSTs and in the ocean. We then discuss a possible feedback to the atmosphere which in turn drives decadal variability in tropopause temperatures as well as LS water vapour. A special analysis focus will be on time lags and the zonal asymmetries, which have been less investigated but are important for understanding the potential underlying mechanisms. We use the F10.7 cm solar radio flux to indicate the solar variability, the Hadley Centre SST analysis (HadISST) (Rayner et al. 2003) and the ocean reanalysis from the European Centre for Medium-Range Weather Forecasts (ECMWF) ocean reanalysis system 4 (ORAS4) from 1958 to 2013 to detect the solar impacts on the Pacific ocean. The Japanese 55-year Reanalysis (JRA-55), one of the most recent reanalysis data, from 1958 to 2013 (Kobayashi et al. 2015; Harada et al. 2016) is used to investigate the atmospheric response. Solar signals in LS water vapour are investigated with the Stratospheric Water and OzOne Satellite Homogenized (SWOOSH) data (Davis et al. 2016). Data and methods are described in Sect. 2. Results are shown in Sect. 3. We first investigate solar signals in the lower atmosphere in Sect. 3.1 which result from the top-down stratospheric pathway. Then the solar responses at the surface and subsurface of the ocean are investigated in Sect. 3.2. In Sect. 3.3, we show ocean feedbacks to the atmosphere. A solar-SST-tropopause connection is addressed in Sect. 3.4. Section 4 summarizes results and discusses possible future research directions.

2 Data and method

2.1 Data

Solar Cycle Index Monthly values of the f10.7 cm solar radio flux (F10.7) index, which is available at NOAA's Space Weather Prediction Center (http://www.swpc.noaa.gov/) are used to represent solar irradiance variations. The F10.7 solar index is closely correlated with solar UV variations, which are essential for the "top-down" mechanism through which solar cycle has impacts on the climate. The data is available since 1947 and a period of 1958–2013 is used in this study to be consistent with the availability of the atmospheric and the oceanic reanalysis data.

Sea Surface Temperatures (SSTs) SSTs are analyzed from the Hadley Centre Sea Ice and Sea Surface Temperature (HadISST) data set (Rayner et al. 2003). It is available from the Hadley Centre website (www.metoffice.gov.uk/hadobs/). This data set is reconstructed from observations since 1870, with a horizontal resolution of 1°. Monthly values for a period of 1958–2013 are selected in this study to be consistent with the availability of the atmospheric and the oceanic reanalysis data.

Ocean Reanalysis The ECMWF ORAS4 data is used to detect solar signals in the ocean. The ORAS4 reanalysis is a product of a combination of model simulation (NEMO ocean model) and quality controlled ocean observations. The ocean model is forced by atmospheric reanalysis fluxes, e.g., ERA-40, ERA-Interim and ECMWF OPS. Observed temperature and salinity profiles (from the Hadley Centre's EN3 data collection (Ingleby and

Huddleston 2007)), as well as altimeter-derived sea level anomalies (from AVISO) are also assimilated. Heat fluxes are adjusted by relaxation using gridded maps of SSTs (from NOAA), and the fresh-water flux is constrained by altimeter global mean sea-levels. The horizontal resolution of the ocean model is approximately 1° near the pole and about 1/3° at the equator, which is refined meridionally down from the pole to the equator. The vertical resolution is varying from 10 m near the surface to 300 m near the bottom, with 42 vertical levels in total. The subsurface temperature, salinity fields as well as ocean heat contents and the depth of the thermocline in ORAS4 have been validated by a comparison with in suite observations and show good agreement with observations in both climatologies and time series (Balmaseda et al. 2013). Zonal currents in the equatorial Pacific in ORAS4 show good agreement in horizontal pattern and vertical structure as well as consistent evolution with observations associated with ENSO (Mogensen et al. 2012).

Stratospheric Water Vapour The SWOOSH is a merged data set for stratospheric water vapour and ozone, with a combination of data from a number of satellites, e.g., SAGE-II/III, UARS HALOE, UARS MLS, and Aura MLS instruments. It is available since 1984. However, there are large amount of missing values before 1991 since there are less satellite instruments on board. The SWOOSH data is gridded to 31 vertical levels from 316 to 1 hPa. Homogenization is done for different measurements by corrections based on their data for their overlap times. Detailed descriptions of the data set can be found in Davis et al. (2016).

The Japanese 55-year Reanalysis (JRA-55) The JRA-55 is analyzed for atmospheric responses to the solar cycle. The JRA-55 is conducted by the Japan Meteorological Agency (JMA). JRA-55 is produced by an atmospheric model with higher spatial resolution (T319L60), using a four-dimensional variational (4D-Var) data assimilation system. Variational Bias Correction (VarBC) is applied for satellite radiances. Many deficiencies has been improved since the first generation of the Japanese reanalysis (Kobayashi et al. 2015). It extends back to 1958, which is coinciding with the time that radiosonde observations in the Arctic became more systematic and regular, and therefore covers more than five decades (Harada et al. 2016) .

Even though reanalysis data are not pure observations, they are the current best estimation of the real atmosphere and provide the best way to investigate temperature and circulation changes over the past decades. JRA-55 is one of the most recent reanalysis. Tropopause temperatures in JRA-55 show extremely good agreement with the GPS-Radio Occultation (GPS-RO) data for their common period from 2001 through 2013 (Fig. S1). Note that the GPS-RO data is not assimilated in JRA-55 and therefore these datasets are independent of each other. The JRA-55 reanalysis, which covers over five decades, is therefore a very suitable data record for analyzing solar signals in tropopause temperatures.

Note that the JRA-55 show a quite weak direct solar signal around the stratopause (Mitchell et al. 2014). However, while the upper stratosphere is less constrained by observations in reanalyses, there is still some uncertainty in the magnitude of solar signals near the stratopause (Mitchell et al. 2015). In the stratosphere and troposphere, the solar signals in JRA-55 show good agreement with other datasets. We have checked that the solar signals shown in this study using the JRA-55 data are consistent with results using the MERRA2 data by taking the same period for analysis (not shown). So, the JRA-55 is a representative dataset for our purpose.

2.2 Methods

Multiple linear regression (MLR), which has been widely used in earlier studies, e.g. (Chiodo et al. 2014; Mitchell et al. 2015; Kodera et al. 2016), is applied here to estimate solar impacts on the atmosphere and the ocean. Observed variability of the climate is a mixture of natural and anthropogenic as well as external and internal influences. MLR is widely used to isolate influences of different factors, such as greenhouse gases (GHGs), the 11-year solar cycle, volcanic aerosols and ENSO. For a time-dependent variable X(t):

$$X(t) = c_1 ENSO(t) + c_2 Solar(t) + c_3 AOD(t) + e(t), \quad (1)$$

where $ENSO(t)$ is an ENSO index, which is the first PC (principal component) of global SST anomalies (HadISST data, after the climatological annual cycle and the long-term trend have been removed); $Solar(t)$ is the F10.7 solar index as described above; $AOD(t)$ is an index of stratospheric aerosols, which was constructed by the Chemistry-Climate Model Initiative (CCMI) project ($ftp://iacftp.ethz.ch/pub_read/luo/ccmi/$); $c_i, i = 1, 2, 3$ are their regression coefficients; and $e(t)$ is the residual term.

For a MLR model, it is essential to assess the statistical significance of the regression coefficients. The statistical significance of a regressed coefficient, e.g., c_2 for solar, can be estimated by a comparison with the standard error (SE), which is defined as:

$$(\mathrm{SE})^2 = \left[\sum_{t=1}^{n} e(t)^2\right] \Big/ \left[(n_{\mathrm{dof}} - 2)\sum_{t=1}^{n} (Solar(t) - \overline{Solar(t)})^2\right], \quad (2)$$

where n is the sample size, $e(t)$ is the residual, and $\overline{Solar(t)}$ is the mean value. $n_{\mathrm{dof}} = n - p - 1$ are the degrees of freedom of the MLR model with p is the number of predictors.

While autocorrelation in the residual leads to an underestimation of the regressed coefficient uncertainties, n_{eff}, which is the effective number of degrees of freedom, it is commonly used instead of n_{dof}, and can be determined by:

$$n_{\mathrm{eff}} = n_{\mathrm{dof}} \frac{1 - r_{\mathrm{a}}}{1 + r_{\mathrm{a}}}, \tag{3}$$

where r_{a} is the lag-1 autocorrelation coefficient (Wigley 2006).

For the estimated coefficients c_2, the test statistics

$$t\_test = \frac{c_2}{SE}, \tag{4}$$

has the Student's t-distribution with $n_{\mathrm{eff}} - 2$ degrees of freedom.

This MLR model is applied to monthly anomalies at each location. Monthly anomalies here are monthly time series with the climatological annual cycle removed. The global mean has also been removed to exclude potential influences from GHGs (Deser et al. 2010). Time lags from 0 to 3 years are used with respect to the solar predictor for estimating potential solar influences in the ocean as well as their subsequent feedbacks to the atmosphere. Note that the QBO influences are not included in the regression analysis since it has little contribution to decadal variability. Sensitivity tests reveal that regression results shown in this study remain the same if the QBO is included in the MLR model, which has also been reported by Gray et al. (2013).

The period from 1958 through 2013 is used for all regression analyses in this study if not stated otherwise. The 1958–2013 period is selected for two reasons: (1) The oceanic observations are more reliable after World War II (Thompson et al. 2008), and (2) the oceanic and atmospheric reanalysis data used in this study, i.e. ORAS4 and JRA-55, are available since 1958. Note that the atmospheric reanalysis data are less reliable before the satellite era, i.e. before 1979. However, a relatively long-term record is very important for detecting solar signals on decadal time scale. Considering the availability, reliability as well as the consistency of the oceanic and the atmospheric data sets, we finally chose the 1958–2013 period for our analyses.

3 Results

3.1 Solar impacts on the atmosphere

Zonal mean signals in the upper stratosphere, i.e., positive temperature anomalies through most of the upper stratosphere and subsequent strengthening of subtropical jets (see Fig. S2), have been well documented as part of the top-down mechanism in previous studies (Gray et al. 2010; Mitchell et al. 2015; Kodera et al. 2016). The anomalous westerlies propagate down to the lower stratosphere and the troposphere (Fig. S2), and project onto a positive NAM which is related to a poleward shift of the jet stream in the Northern Hemisphere (NH) (Matthes et al. 2006; Kodera et al. 2016). Here we mainly focus on the horizontal pattern of such zonal wind anomalies during their downward propagation from the lower stratosphere to the troposphere in the NH, which has been less investigated in previous studies.

Figure 1 shows longitude–latitude distributions of solar signals in zonal wind at 50, 100, 300 and 500 hPa, analyzed from monthly anomalies. Also shown in Fig. 1 are climatological values of the zonal wind, with the purpose to demonstrate the relationship between solar related wind anomalies and the basic state of the air flow. At 50 hPa (Fig. 1a), the anomalous westerlies are evident in mid-latitudes and subpolar while easterly anomalies can be seen in lower latitudes, which resembles the NAM (Thompson and Wallace 2000; Baldwin and Dunkerton 2005; Kodera et al. 2016). Note that the anomalous westerlies in mid-latitudes and subpolar are not zonally uniform, as also indicated by Kodera et al. (2016), but have a stationary planetary wave structure. These westerly anomalies in the mid-latitudes show local maxima over the Asian-Pacific and the North American-Atlantic jet-stream regions, whereas the basic state of zonal winds are relatively strong (see contour lines in Fig. 1a).

At lower altitudes, solar associated westerly anomalies shift slightly to the subpolar regions, while the easterly anomalies extend to mid-latitudes (Fig. 1b). This is consistent with the transition behavior of the NAM from a monopole in the subpolar stratosphere (with a weak subtropical extrema of opposite sign) to a dipole in the troposphere straddling approximately 45°N with each extrema of roughly equal magnitude. At the same time, zonal asymmetry in the basic state of the air flow (contour lines in Fig. 1b–d) as well as solar related westerly anomalies mentioned above are more prominent in the troposphere (Fig. 1b–d). In particular, it seems that anomalous westerlies propagate to lower latitudes from the northwest to the southeast of the North Pacific (Fig. 1b–d). According to the planetary wave propagation theory (Hoskins and Ambrizzi 1993), the basic state flow impacts the wave propagation. The Asian-North Pacific jet region, where the westerly winds are particularly strong (as revealed by contour lines in Fig. 1b–d), provides a potential pathway (or waveguide) for planetary waves to propagate (Hoskins and Ambrizzi 1993). The anomalous westerlies in mid-latitudes might then propagate to lower latitudes over the Pacific as seen in Fig. 1b–d, following the Asian-North Pacific pathway.

To further indicate the downward and meridional propagation of solar signals over the Asia-North Pacific region, the latitude-height cross sections of solar regressed zonal wind anomalies averaged for the western Pacific section are shown in Fig. 2 (top). Solar signals over the western Pacific are more significant than the zonal mean (Fig. S2), and the meridional propagation from high to mid latitude is more evident. While taking a shorter period of 1979–2010

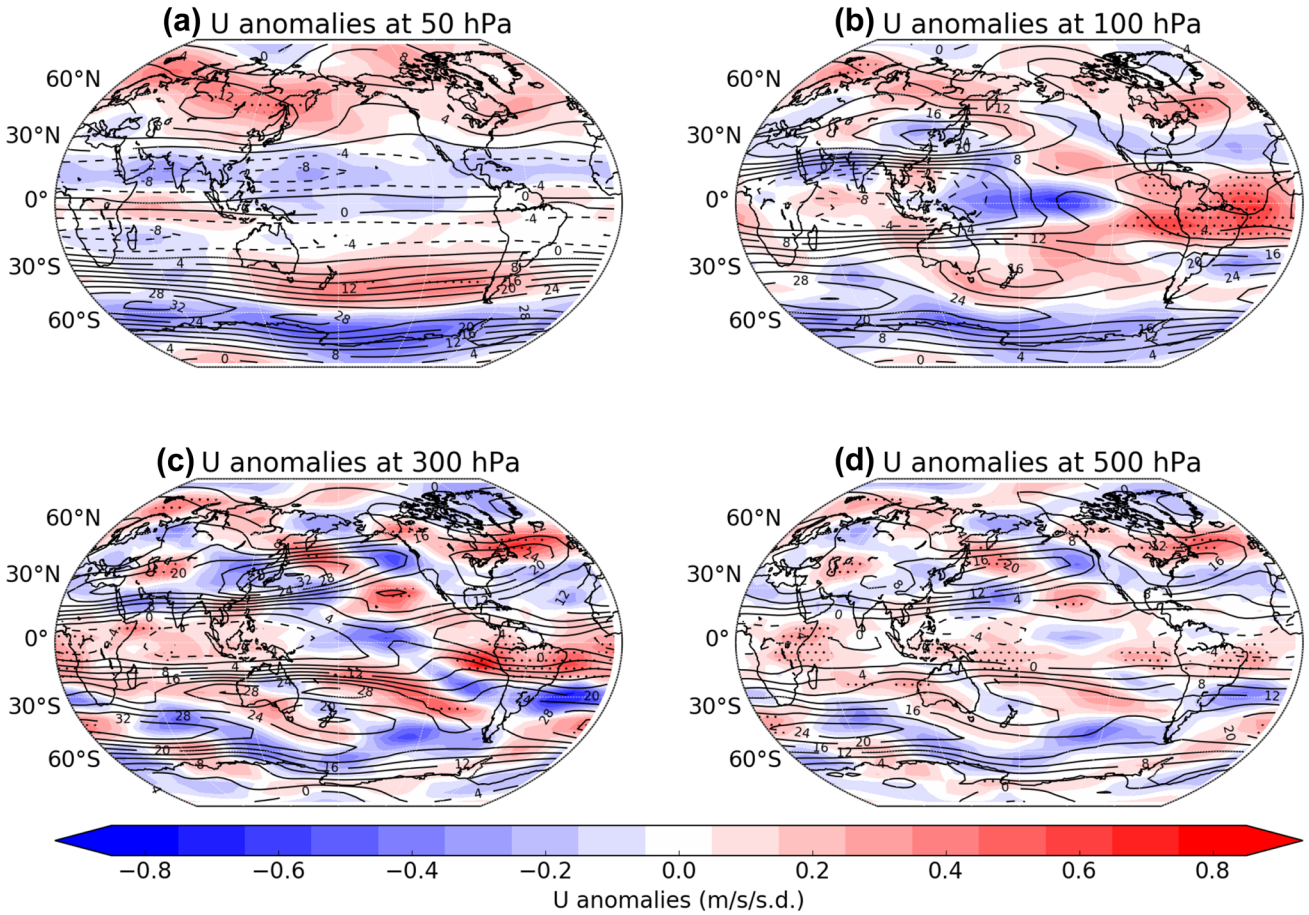

Fig. 1 Solar regressed anomalies of zonal winds at **a** 50, **b** 100, **c** 300 and **d** 500 hPa using the JRA-55 reanalysis (1958–2013). Contour lines are climatological values (averaged over 1958–2013) of zonal wind at the corresponding pressure levels. Areas over 90% statistically significance level are stippled. Autocorrelation effects has been excluded for the statistic test

for analysis as previous studies (Kodera et al. 2016), signals shown in Fig.2 (top) are stronger and more significant (Fig. S3). Such downward and meridional propagation of solar associated anomalous westerlies can also be confirmed by the month-dependent regressed results (Fig. 2, bottom). Westerly anomalies associated with the 11-year solar cycle are strongest in December in the middle stratosphere, while the tropospheric signals are more significant in January. This indicates a downward propagation of solar signals from the stratosphere to the troposphere which takes about 1 month.

Figure 3 further shows solar associated zonal wind, as well as meridional wind and geopotential height anomalies at 850 hPa to give an overview of circulation changes near the surface. Over the western North Pacific, statistically significant anomalous westerlies exist between 30°N and 60°N with anomalous easterlies on both sides (Fig. 3a), while northward meridional wind anomalies exist around 30°N beside the eastern coast of Asia (Fig. 3b). All these zonal and meridional wind anomalies are in balance with anticyclonic circulations near 30°N beside the eastern coast of Asia, which can be confirmed by the anomalous geopotential heights (Fig. 3c). Positive geopotential height anomalies can be seen over the western North Pacific while anomalous low geopotential heights are evident over the northern and eastern part of the Pacific.

Also interesting in Fig. 3 are the anomalous westerlies over the equatorial western Pacific (Fig. 3a). Recent studies have reported that extratropical anomalies like the NAM could influence the tropics and lead to a burst of westerlies over the equatorial western Pacific through intensified cold surges (Nakamura et al. 2007) or interactions between tropospheric eddies and the mean-flow (Chen et al. 2014). Solar induced NAM-like zonal wind anomalies might therefore result in westerly anomalies over the equatorial western Pacific through the above mentioned mechanisms. While the near surface circulation is closely coupled to the ocean, wind anomalies in the mid-latitudes as well near the equator influence the surface temperatures significantly and will be discussed in Sect. 3.2.

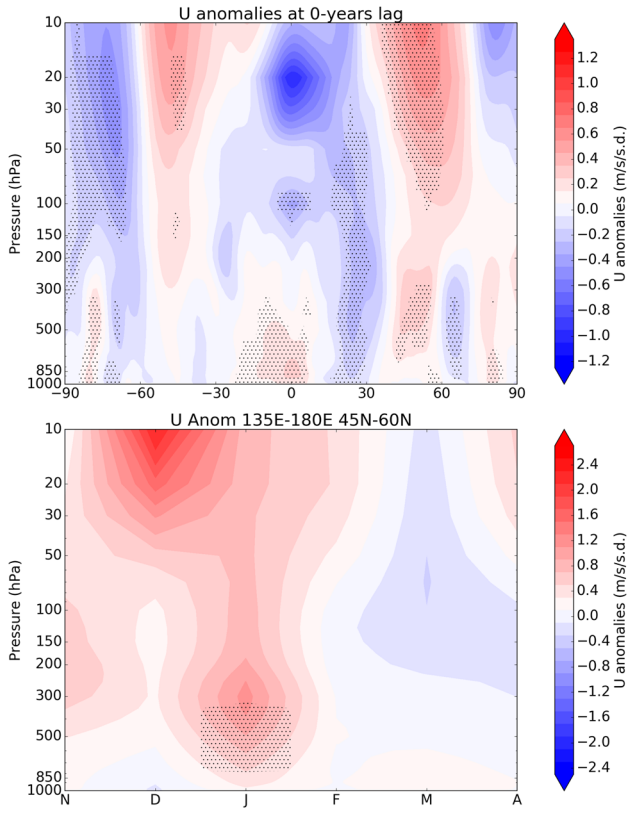

Fig. 2 (Top) Latitude-height cross sections of solar regressed zonal wind anomalies averaged over the western Pacific (135° E–180°E) using the JRA-55 reanalysis (1958–2013). (Bottom) Solar regressed zonal wind anomalies (averaged for the region 45°N–60°N, 135° E–180°E) distributed at different pressure levels for different months using the JRA-55 reanalysis (1958–2013). Areas over 90% statistically significance level are stippled. Autocorrelation effects has been excluded for the statistic test

3.2 Solar signals at the surface and in the ocean

Figure 4 shows global regression pattern of SST anomalies (colour filled contours, from HadISST) onto the solar F10.7 time series with different time lags in years (0–3 years) for the period from 1958 through 2013. Shown together are surface wind (1000 hPa) anomalies associated with the solar cycle (arrows, from the JRA-55 reanalysis). Wind anomalies at the surface associated with the solar cycle are similar to that at 850 hPa as shown in Fig. 3, with anomalous anticyclonic/cyclonic circulations over the western/eastern part of the Pacific in mid-latitudes and westerly anomalies over the equatorial western Pacific (Fig. 4a). Anomalous anticyclonic circulation brings warm water from the subtropics to the mid-latitudes beside the western coast of the Pacific and cold water from higher to lower latitudes in the central Pacific, which subsequently lead to positive SST anomalies in the western North Pacific and negative SST anomalies in the central part of the North Pacific (Fig. 4a). At the same time, anomalous cyclonic circulations occur over the eastern North Pacific (Fig. 4a), which bring warm water from the subtropics to the mid-latitudes along the coastline of North America and cause positive SST anomalies beside the east coast of the Pacific (Fig. 4a). In the tropics, anomalous westerlies or a weakening of the trade winds over the western Pacific dampen the heat transport from the central to the western Pacific, and therefore lead to warm SST anomalies in the central Pacific and cold anomalies in the western Pacific (Fig. 4a). Westerly anomalies are confined to the central Pacific, while weak easterly anomalies exist in the eastern Pacific, which lead to weak and insignificant negative SST anomalies in the cold tongue region.

All these signals are consistent with common features, i.e. positive SST anomalies over the central Pacific and the western coast of North America and anomalous cold SSTs over the cold tongue region, associated with the solar cycle as described in the Introduction (Tung and Zhou 2010; Gray et al. 2013; Kodera et al. 2016). Note that the method in this study (MLR applied to monthly anomalies) is slightly different to earlier studies (MLR or CMD applied to DJF SSTs) (Tung and Zhou 2010; Gray et al. 2013; Kodera et al. 2016), which makes our results slightly different compared to previous studies, i.e., the positive anomalies shown in the central Pacific (Fig. 4a) are stronger and more significant than in previous studies, while the negative anomalies in the cold tongue region are weaker and not that significant as shown previously. The time period of analysis could be another reason for the described descrepancies. We selected the period of 1958–2013, as described in Sect. 2, while earlier studies used a longer period from 1870s to 2000s (Tung and Zhou 2010; Misios and Schmidt 2012; Kodera et al. 2016). Choosing a longer period (1900–2010) as shown in supplementary Fig. S4, SST anomalies associated with the 11-year solar cycle are weaker than that shown in Fig. 4a–d and more consistent with previous studies (Tung and Zhou 2010; Misios and Schmidt 2012; Kodera et al. 2016).

Solar related SST anomalies resemble the ENSO associated SST pattern. However, anomalous SSTs in the cold tongue region are much weaker or even negative, and therefore different from the conventional ENSO pattern. The detected signals by definition could not be a conventional ENSO since the ENSO predictor is already included in the MLR model and all variances related to ENSO hence goes to this predictor. The solar associated SST pattern, as also mentioned in recent studies (Kodera et al. 2016; Huo and Xiao 2017), is more similar to the so-called El Niño Modoki event. The El Niño Modoki is the second EOF (empirical orthogonal function) mode of detrended tropical SST anomalies (Ashok et al. 2007). Fig. 4e, f show SST anomalies associated with the conventional ENSO and the El Niño Modoki events (see Fig. 4 caption for definitions of ENSO and El Niño Modoki indices). Anomalous warm SSTs occur

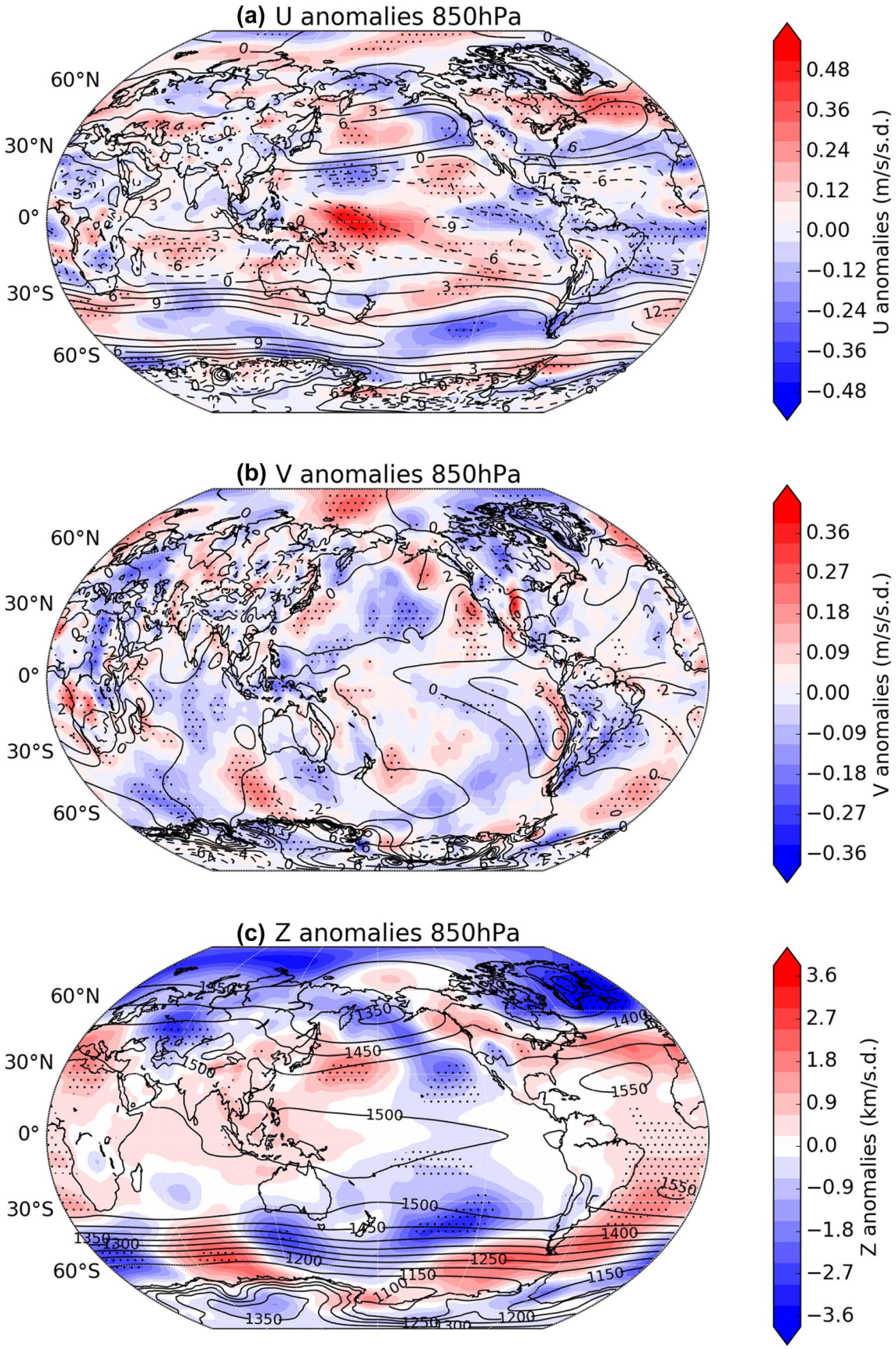
(a) U anomalies 850hPa
60°N
30°N
0°
30°S
60°S
0.48
0.36
0.24
0.12
0.00
−0.12
−0.24
−0.36
−0.48
U anomalies (m/s/s.d.)
(b) V anomalies 850hPa
60°N
30°N
0°
30°S
60°S
0.36
0.27
0.18
0.09
0.00
−0.09
−0.18
−0.27
−0.36
V anomalies (m/s/s.d.)
(c) Z anomalies 850hPa
60°N
30°N
0°
30°S
60°S
3.6
2.7
1.8
0.9
0.0
−0.9
−1.8
−2.7
−3.6
Z anomalies (km/s.d.)

◂**Fig. 3** Solar regressed anomalies of **a** zonal wind, **b** meridional wind and **c** geopotential height at 850 hPa using the JRA-55 reanalysis (1958–2013). Contour lines are climatological values (averaged over 1958–2013) of **a** zonal wind, **b** meridional wind and **c** geopotential height at the corresponding pressure level. Areas over 90% statistically significance level are stippled. Autocorrelation effects has been excluded for the statistic test

in the central Pacific for an El Niño Modoki event, while anomalous cold SSTs dominate in the western Pacific and cold tongue region (Fig. 4f). The main differences between the El Niño Modoki and the conventional El Niño are the negative SST anomalies in the cold tongue region, which can not be seen in the conventional El Niño (Fig. 4e). A wavelet analysis (Torrence and Compo 1998) indicates that the power spectrum of the El Niño Modoki index (EMI) performs statistically significant decadal peak at about 12 years while the conventional ENSO index, however, shows no significant decadal variability (Fig. S5). This further confirms that the SST anomalies associated with the solar cycle are more likely related to the El Niño Modoki rather than the conventional ENSO.

Note that the solar associated SST pattern is also similar to the Pacific Decadal Oscillation (PDO), which is an internal variability mode of the climate system. The PDO has a significant decadal peak and plays an important role in modulating decadal variability of tropopause temperatures (Wang et al. 2016). While the El Niño Modoki and the PDO are closely coupled on decadal timescales, it is hard to completely separate them. Since the SST pattern is more similar to the El Niño Modoki than the PDO (weak negative SST anomalies in the eastern Pacific, which does not exist in PDO events), we use the El Niño Modoki for solar associated SST anomalies in this study.

From the descriptions above, we got a clear feature of solar associated SST anomalies that resemble the El Niño Modoki pattern. A key issue is the positive SST anomaly in the equatorial central Pacific. One reason for this positive SST anomaly is possibly related to a burst of westerly zonal wind anomalies over the western Pacific, which might at least in part result from anomalous westerlies in mid-latitudes associated with the top-down mechanism as described in Sect. 2. As indicated by recent studies, there might be another reason related to cyclonic circulation over the eastern North Pacific and subsequent positive SST anomalies along the coastline of North America in the subtropics (Huo and Xiao 2017; Xie et al. 2016; Garfinkel 2017). Such subtropical SST anomalies persist into spring through thermodynamical air–sea interactions (Alexander et al. 2010), and force westerly zonal wind anomalies over the equatorial western Pacific in the following winter, which is the so-called seasonal footprinting mechanism (SFM) (Vimont et al. 2001). According to the SFM, anomalies in SST and circulation over the North Pacific may influence tropical regions and inspire an ENSO evolution (Xie et al. 2016; Garfinkel 2017). However, such an extratropical-to-tropical mechanism is related to very complex atmospheric and oceanic processes and awaits further investigations with extra observations and/or model simulations. It is therefore out of the scope of this study since we are mainly focusing on solar signals in the ocean and their feedbacks to the atmosphere.

Now we consider solar impacts in the years following a solar maximum. Associated with anomalous positive SSTs in the central Pacific and anomalous negative SSTs in the western and eastern Pacific, the zonal temperature gradient and subsequent circulation and heat transport are changed. In the western Pacific, the zonal temperature gradient is reduced. While the zonal temperature gradient is the main driver of the Walker circulation, easterly trade winds are dampened over the western Pacific as seen from anomalous westerlies over this region in Fig. 4b. A weaker Walker circulation, which means less transport of heat from the central Pacific to the western Pacific, leads to warmer SSTs in the central Pacific and colder SSTs in the western Pacific. In the eastern Pacific, the situation is different. Though not significant, anomalous negative SSTs exist in the eastern Pacific, which means enhanced zonal temperature gradient from the eastern to the central Pacific. Weak easterly anomalies therefore persist in the eastern Pacific and lead to a convergence of surface water and heat transport in the central Pacific. SST anomalies in the equatorial Pacific are then enhanced through the zonal advection feedback of the Bjerknes feedback (Bjerknes 1969) and result in a clear El Niño Modoki-like evolution in the equatorial Pacific during the following 2 years after solar maxima (Fig. 4a–c). At about 2 years after the solar maximum, solar related positive SST anomalies in the equatorial central Pacific reach their maximum and an El Niño Modoki-like pattern can be clearly depicted (Fig. 4c). With longer time delay, solar related SST and near surface wind signals decay (Fig. 4d). A very similar time lag also exists in the North Atlantic (Scaife et al. 2013), where a positive NAO-like pattern is formed 2 years after the solar maximum which synchronizes with the solar cycle (Thiéblemont et al. 2015).

As mentioned in the introduction, solar signals in SSTs should also be detectable in the subsurface ocean. The responses in oceanic currents and circulations to the solar cycle are important in order to fully understand the underlying mechanisms. However, because there are not enough observations in the ocean, most research about solar signals in the subsurface ocean are based on model simulations (Misios and Schmidt 2012; Misios et al. 2016) except for White et al. (1997), which analyzed solar signals through bathythermograph (BT) upper ocean temperature profiles from 1955 to 1994. This study gives the first investigation of solar signals in the subsurface ocean using the recently available ORAS4 oceanic reanalysis (Fig. 5). Statistically

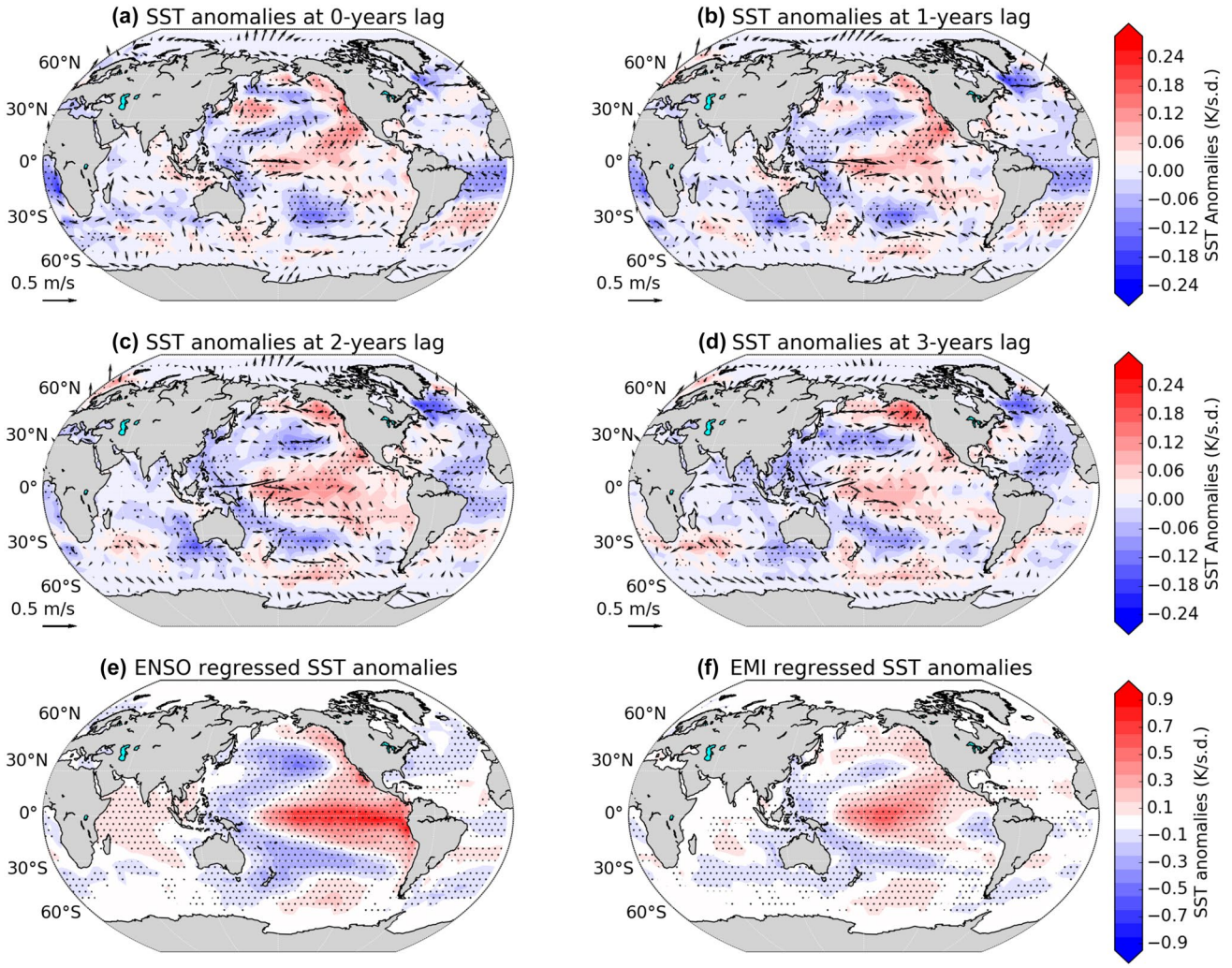

Fig. 4 Up, **a–d** Solar regressed anomalies of SSTs using the HadISST data (colour) and horizontal winds (vectors) at 1000 hPa using the JRA-55 reanalysis (1958–2013). Time lags of 0, 1, 2, 3 years are considered while doing the regression. Bottom, **e, f** The regression pattern of SST anomalies data regressed on the **e** ENSO and **f** El Niño Modoki indexes using the HadISST data for the period 1958–2013. The El Niño Modoki index (EMI) used here is defined as $T_A - 0.5 * T_B - 0.5 * T_C$ (**a** 165° E–140°W, 10°S–10°N; **b** 110° W–70° W, 15°S–5°N; **c** 125° E–145°E, 10°S–20°N). Areas over 90% statistically significance level are stippled. Autocorrelation effects has been excluded for the statistic test

significant positive ocean temperature anomalies in the central Pacific persist from the surface to about 150 m depth. With longer time delay, the near surface temperature anomalies extend from the western part of the central Pacific to the east and reach their maximum after about 2 years. This confirms the result of a previous study using Coupled Model Inter-Comparison Project (CMIP5) models (Misios et al. 2016), which found solar signals in the subsurface of the ocean until about 150 m and peaking at about 2 years after the solar maximum. Also interesting is that the strongest and statistically significant positive temperature anomalies occur between 50 and 150 m depth. The strongest signal exists below the surface suggesting a dynamical cause and amplification mechanism in the ocean instead of radiative reasons. This can be further confirmed by solar signals in subsurface ocean currents as shown in Fig. 5 (right column).

As shown in Fig. 4, anomalous positive temperatures at the surface of the central Pacific reduce/strengthen zonal temperature gradients in the western/eastern Pacific, and lead to anomalous westerlies over the western Pacific and easterly anomalies over the eastern Pacific in the atmosphere. Changes in the atmospheric circulation then drive surface ocean currents, with anomalous eastward/westward currents in the western/eastern Pacific (Fig. 5b). Sea water converges in the central Pacific and then sinks to the subsurface (or less upwelling) due to the Ekman feedback of the Bjerknes feedback (Bjerknes 1969). The oceanic water then diverges at about 200 m depth and results in anomalous

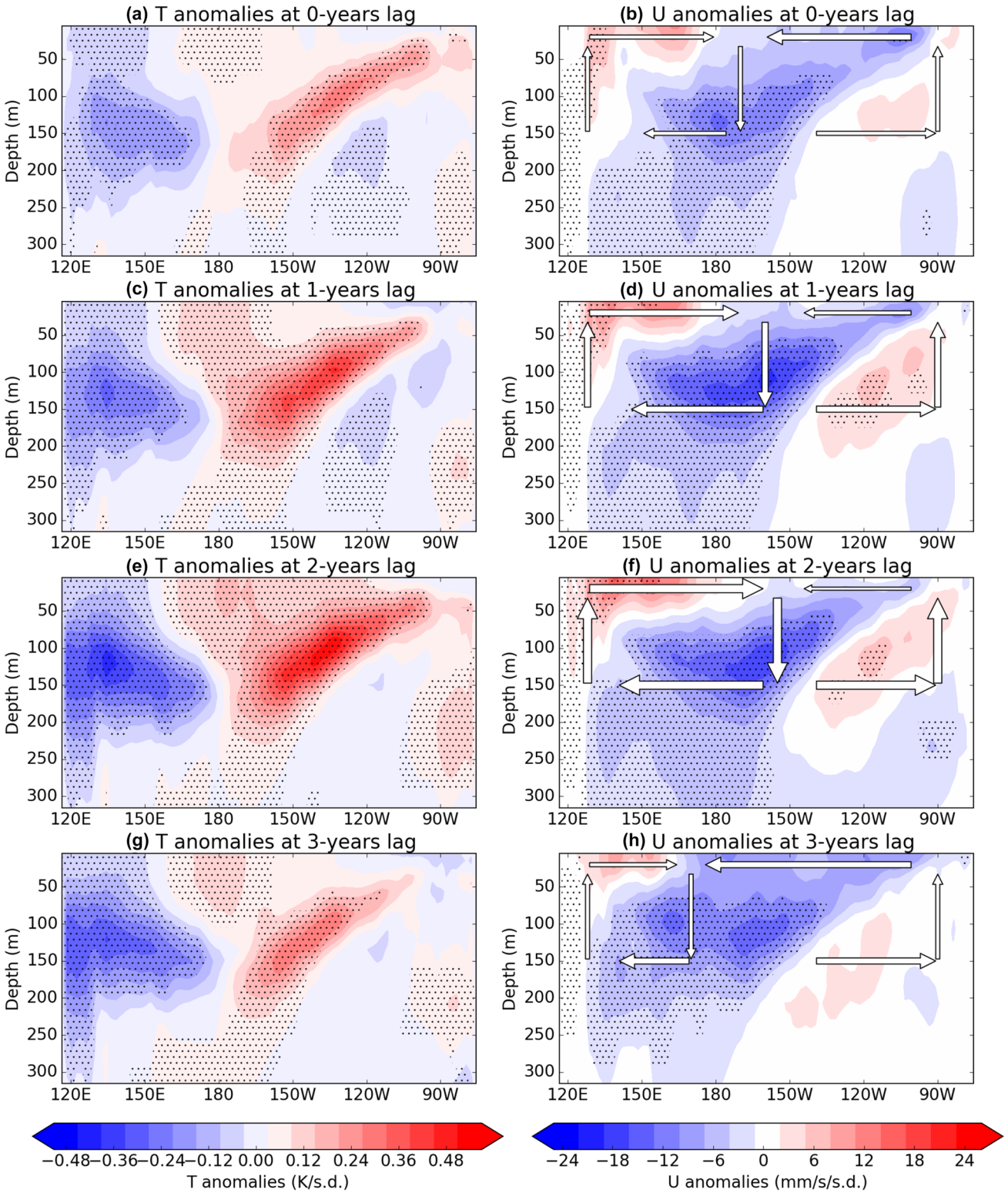

Fig. 5 Solar regressed oceanic (left) temperature and (right) zonal flow anomalies in the tropical Pacific basin using the ECMWF ORAS4 data for the period 1958–2013. Time lags of 0, 1, 2, 3 years are considered while doing the regression. Areas over 90% statistically significance level are stippled. Autocorrelation effects has been excluded for the statistic test. Arrows indicate the schematic oceanic circulation responses to the solar cycle based on the divergence and convergence of zonal flow and the continuity of the fluid

westward/eastward current in the subsurface of the eastern/western Pacific (Fig. 5b) due to the fluid continuity, which leads to negative ocean temperature anomalies in these regions (Fig. 4a). These anomalous currents lead to enhanced upwelling near the western and eastern coasts of the Pacific (Fig. 5b). The stronger upwelling brings cold water from the subsurface to the surface and contributes to the negative SST anomalies at the surface of the western and eastern Pacific near the coasts (Figs. 4a and 5a), while anomalous eastward/westward currents near the surface in the western/eastern Pacific bring warm water to the surface of the central Pacific and therefore provide positive feedbacks to the positive SST anomalies in that area (Figs. 4a and 5a). The solar signals in ocean temperature and currents in the subsurface of the ocean are hence amplified by such a positive feedback (Fig. 5c, d) and peak at a time lag of about 2 years (Fig. 5e, f). With longer time lags, anomalous temperatures and currents decay (Fig. 5g, h), which is consistent with signals at the surface (Fig. 4d).

Now, we provide a summary of the heat budget near the surface of the Pacific ocean with an analysis of the heat budget of the tropical basin. Temperatures near the ocean surface are determined by a balance between net radiation (shortwave and longwave), sensible and latent heat flux, as well as ocean dynamical heat transport. Fig. 6 shows solar signals in the downward solar radiation (DSWRF), latent (LHTFL) and sensible heat flux (SHTFL) as well as heat transport (HT) anomalies. The downward solar radiation, sensible and latent heat flux are from the JRA-55 reanalysis. The heat transport (HT) shown in Fig. 6 is the ocean heat flux divergence (horizontal only here!) advected by the resolved currents, which is calculated by a vertical integration of $\nabla(uT)$ from the surface to 30 m depth of the ocean (DiNezio et al. 2009) based on the ORAS4 data. A depth of 30 m is selected here since this is approximately the depth of the mixed layer in the equatorial Pacific. The mixed layer exchanges energy with the surface rapidly and shares similar temperature variations with the surface. The depth of the mixed layer determines how fast the surface ocean temperature can be changed in response to radiative heating. The evolution of all signals in Fig. 6 is similar to those shown in Figs. 4 and 5, i.e., they develop during the first 1–2 years and peak at about 2 years after the solar maximum and then decay. Therefore, we only show solar signals at 0 and 2 years lag in Fig. 6.

The climatological solar radiation over the eastern and central Pacific is stronger than that over the western Pacific region, since the cloud coverage is larger over the western Pacific and the Maritime Continent and reflects more solar radiation back to space (not shown). The enhanced solar radiation during solar maximum should be more significant over the eastern and central Pacific than over other regions if the cloud coverage over these regions does not change. However, Fig. 6 shows that the enhanced solar radiation is strongest over the western Pacific and Maritime Continent, while the solar radiation decreases over the central Pacific. 2 years after the solar maximum, the decreased solar radiation over the central Pacific reaches its maximum (Fig. 6b). Such changes in solar radiation could be related to tropospheric circulation and subsequent cloud coverage changes instead of a direct response to the solar cycle. The latent heat flux and sensible heat flux, however, show significant negative/positive anomalies over the western/central and eastern Pacific as shown in Fig. 6c, which indicate that the ocean releases more energy to the atmosphere over the central and eastern Pacific because of anomalous positive temperatures in these regions (Fig. 4). Again, all signals maximize 2 years after the solar peak years (Fig. 6d). In summary, it seems that changes in radiation, latent heat flux and sensible heat flux are the result rather than the cause of the positive SST anomalies over the central Pacific.

Associated with the near surface wind and ocean current anomalies (Figs. 4 and 5), the westward heat transport across the Pacific becomes weaker, which means positive anomalies and heat convergence in the western part of the central Pacific, due to weaker easterly surface winds and near surface ocean currents. With longer time delay, the positive anomalies of HT become stronger and more significant in the eastern part of the central Pacific. Positive HT anomalies in the eastern part of the central Pacific are also the effect of a weakening of the meridional HT from the equator to the extra-tropics (not shown). Also noteworthy are the negative HT anomalies in the eastern Pacific near the coastline of Peru, which are getting stronger during the first 2 years after the solar peak years. These positive/negative HT anomalies contribute to the positive/negative SST anomalies in the central/eastern Pacific. Combined with the radiative signals described above, it is obvious that the dynamical heat transport rather than the radiative heating is the reason for SST anomalies in the equatorial Pacific. Our results differ from a recent study, which showed that solar signals in SSTs are mainly caused by radiative effects of high clouds (Huo and Xiao 2017).

3.3 Ocean feedbacks to the tropopause and lower stratospheric water vapour

So far, we have investigated solar signals in SSTs as well as in the oceanic subsurface. A positive feedback is suggested by the interaction between surface ocean temperature anomalies and anomalous ocean currents, which lead to lagged solar related signals in the ocean maximizing at about 2 years. At the same time, such lagged oceanic anomalies can potentially influence the atmosphere again, since SSTs are the main driver of convection and atmospheric circulation in

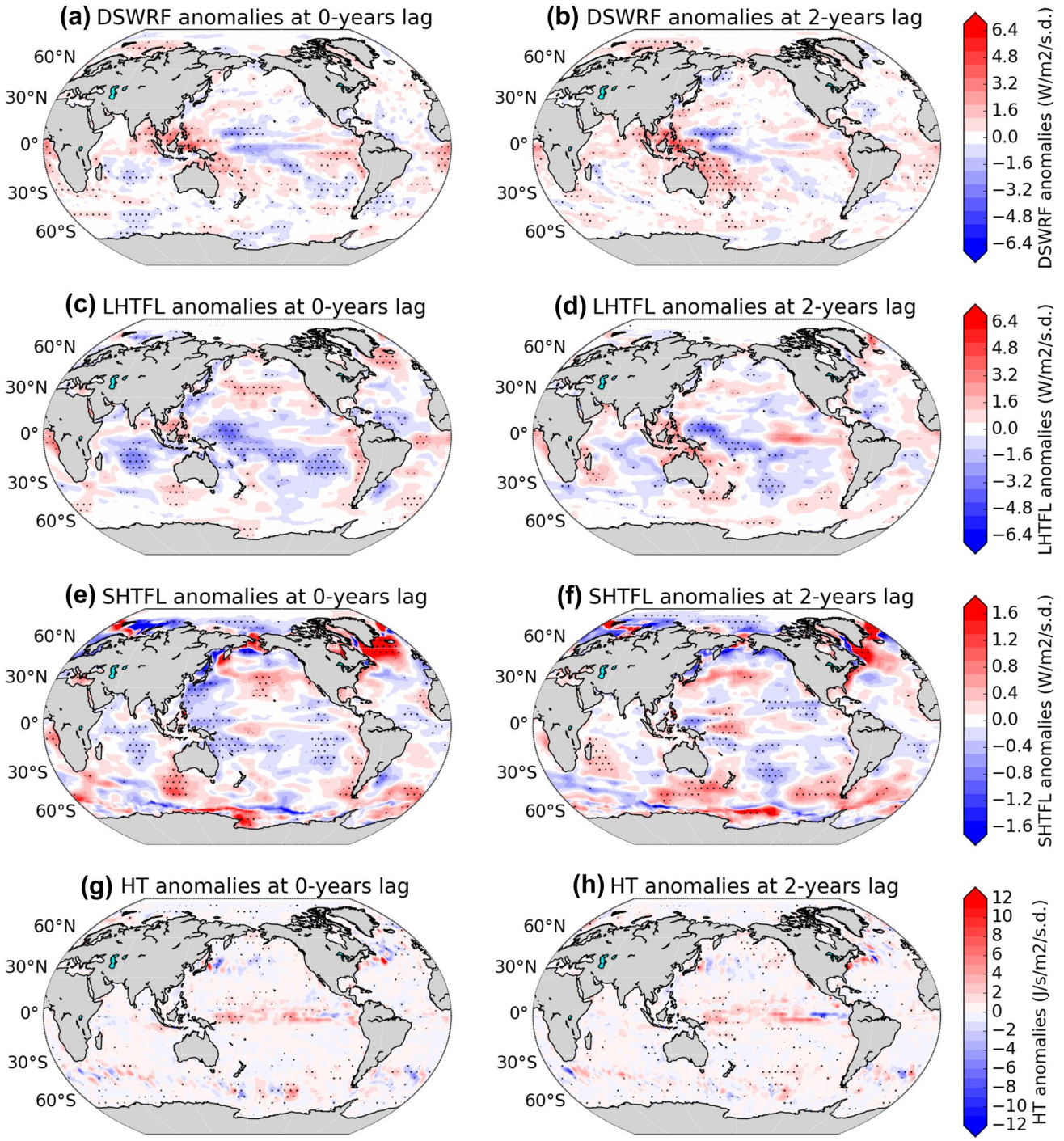

Fig. 6 Solar regressed anomalies of (top-bottom) downward short wave radiative flux (DSWRF), latent heat flux (LHTFL), sensible heat flux (SHTFL) and heat transport (HT) for the period 1958–2013, with time lags of (left) 0 and (right) 2 years. The heat transport was calculated by temperature and wind data from the ECMWF ORAS4. Areas over 90% statistically significance level are stippled. Autocorrelation effects has been excluded for the statistic test

the tropics. We now investigate impacts of the solar-induced SST signals to the atmosphere.

As shown in Fig. 4, the solar cycle leads to positive SST anomalies together with wind convergence over the central Pacific, which are favourable conditions for enhanced convection. Fig. 7 shows solar regressed anomalies in high cloud coverage. More high clouds can be seen over the central Pacific while less clouds are visible over the western

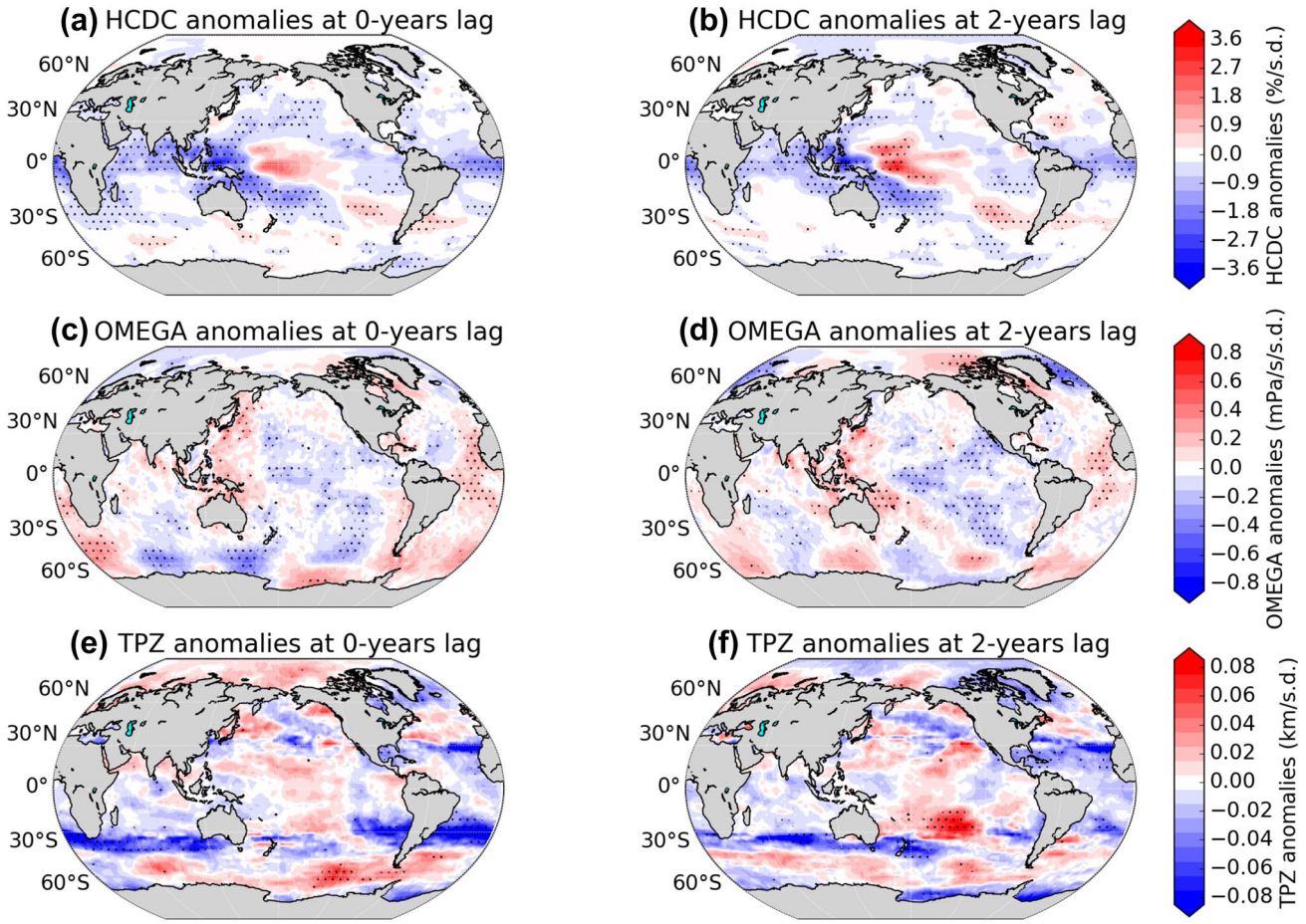

Fig. 7 Solar regressed anomalies of (top-bottom) the frequency of high clouds, vertical velocity in pressure at 100 hPa and tropopause height using the JRA-55 reanalysis for the period 1958–2013, with time lags of (left) 0 and (right) 2 years. Areas over 90% statistically significance level are stippled. Autocorrelation effects has been excluded for the statistic test

and eastern Pacific. This helps to explain the solar radiation changes associate with the solar cycle in Fig. 6a. This indicates a direct response of convection to positive/negative SST anomalies and wind convergence/divergence over these regions. As reported in previous studies, a shift of the location in SST anomalies will change the response pattern in the atmosphere. The corresponding pattern in high clouds shown here, which indicates changes of convection and precipitation, is consistent with the El Niño Modoki associated precipitation anomalies as reported in previous work (Yeh et al. 2009). Such changes in surface winds and convection modulate the Pacific branch of the Walker circulation. Also shown in Fig. 7 are the changes in vertical motion at 100 hPa (near the tropopause) associated with the solar cycle. Note that negative values indicate enhanced vertical motion. Vertical motion is significantly enhanced over the central Pacific (Fig. 7c) and indicates an enhanced upward branch of the Walker circulation. Due to fluid continuity, the upward air flow diverges near the tropopause and moves towards the western and eastern Pacific. The air then sinks to the western and eastern Pacific and might provide a positive feedback to the near surface SST and wind anomalies due to its modulation of the Walker circulation. With longer time lags, signals in SSTs, surface wind (Fig. 4) and deep convection (shown as high clouds coverage here in Fig. 7) become stronger and reach their maximum at the lag of about 2 years. After 2 years, all high cloud and vertical motion anomalies decay (not shown) due to reduced SST anomalies (Fig. 4d). Such a positive feedback in the atmosphere, together with the positive feedback as addressed in Sect. 3.2 through oceanic currents and heat transport, provide a mechanism for the amplification of solar signals in the atmosphere and the ocean.

Enhanced deep convection as well as enhanced vertical motion lift the tropopause. The bottom panel of Fig. 7 shows tropopause height anomalies related to the solar cycle. It is evident that the tropopause height is getting higher during solar maximum years over the central Pacific (Fig. 7e), maximizing at about 2 years (Fig. 7f). At the same time, as expected from the lifted tropopause, tropopause temperatures are decreasing over the central Pacific

region, which can be seen clearly in Fig. 8. On the other hand, low tropopause heights and positive tropopause temperature anomalies are shown over the western and eastern Pacific, because of less convection (Fig. 7a) and weaker vertical motion (Fig. 7c) over these regions. It is noteworthy that tropopause temperature anomalies associated with the 11-year cycle have a clear zonally asymmetric pattern (Fig. 8a). This zonally asymmetric pattern is consistent with previous studies, which show tropopause temperature responses to tropical SSTs (Garfinkel et al. 2013a; Fu 2013; Hu et al. 2014; Wang et al. 2016). This suggests that solar signals in tropopause temperatures are partly a subsequent effect of solar related SST anomalies. This can also be confirmed by the time evolution of solar signals shown in Fig. 8. With longer time lags, solar signals in tropopause temperatures strengthen (Fig. 8b) and peak at the time lag of about 2 years (Fig. 8c) and decay afterwards (Fig. 8d). This indicates a consistent evolution with the SST anomalies in Fig. 4.

3.4 A Solar-SST-TPT link

The connection between SST modes, e.g. ENSO and El Niño Modoki, and tropical tropopause temperatures as well as LS water vapour has been well established in previous studies (Randel et al. 2009; Xie et al. 2012; Garfinkel et al. 2013b; Xie et al. 2014; Wang et al. 2016; Ding and Fu 2017; Garfinkel et al. 2018). Solar signals in tropopause temperatures and LS water vapour, however, have been less investigated in the past (Schieferdecker et al. 2015). Results presented in this study suggest a possible connection of the solar cycle, SSTs and TPTs on decadal timescales. The relationship between the 11-year solar cycle, the El Niño Modoki index, tropical tropopause temperatures and the LS water vapour are shown in Fig. 9. To clearly show their relationship on decadal timescales, all time series have been band-pass filtered between 9 and 13 years. During the past 6 solar cycles, the solar F10.7 cm, overall, is leading the EMI (see definition in the Methods section) by about 16 months with a correlation of about 0.58 (Fig. 9a). Note that the exact lag time between

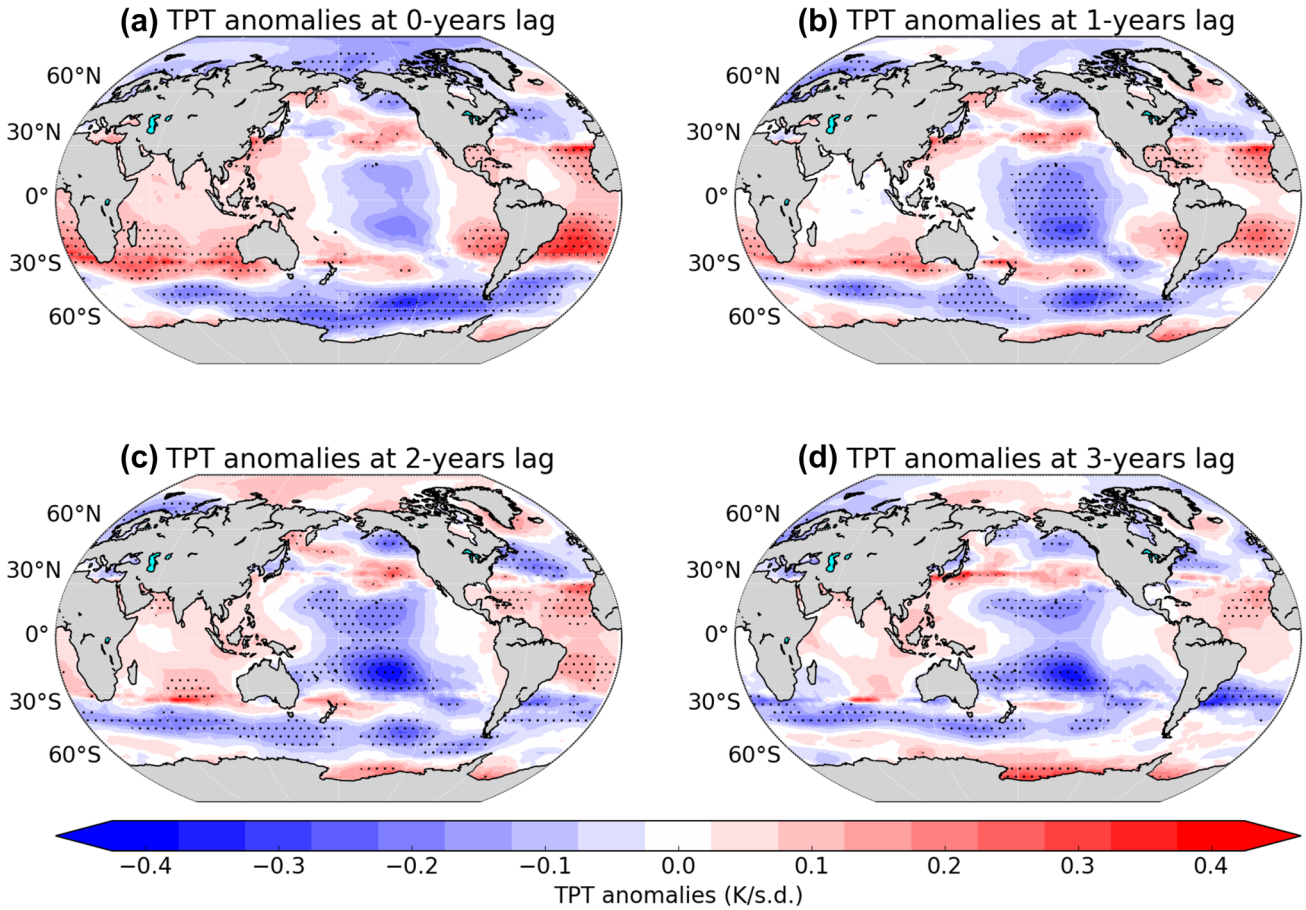

Fig. 8 The regression pattern of tropopause temperature anomalies associated with solar cycle using the JRA-55 reanalysis for the period 1958–2013. Time lags of 0, 1, 2, 3 years are considered while doing the regression. Areas over 90% statistically significance level are stippled. Autocorrelation effects has been excluded for the statistic test

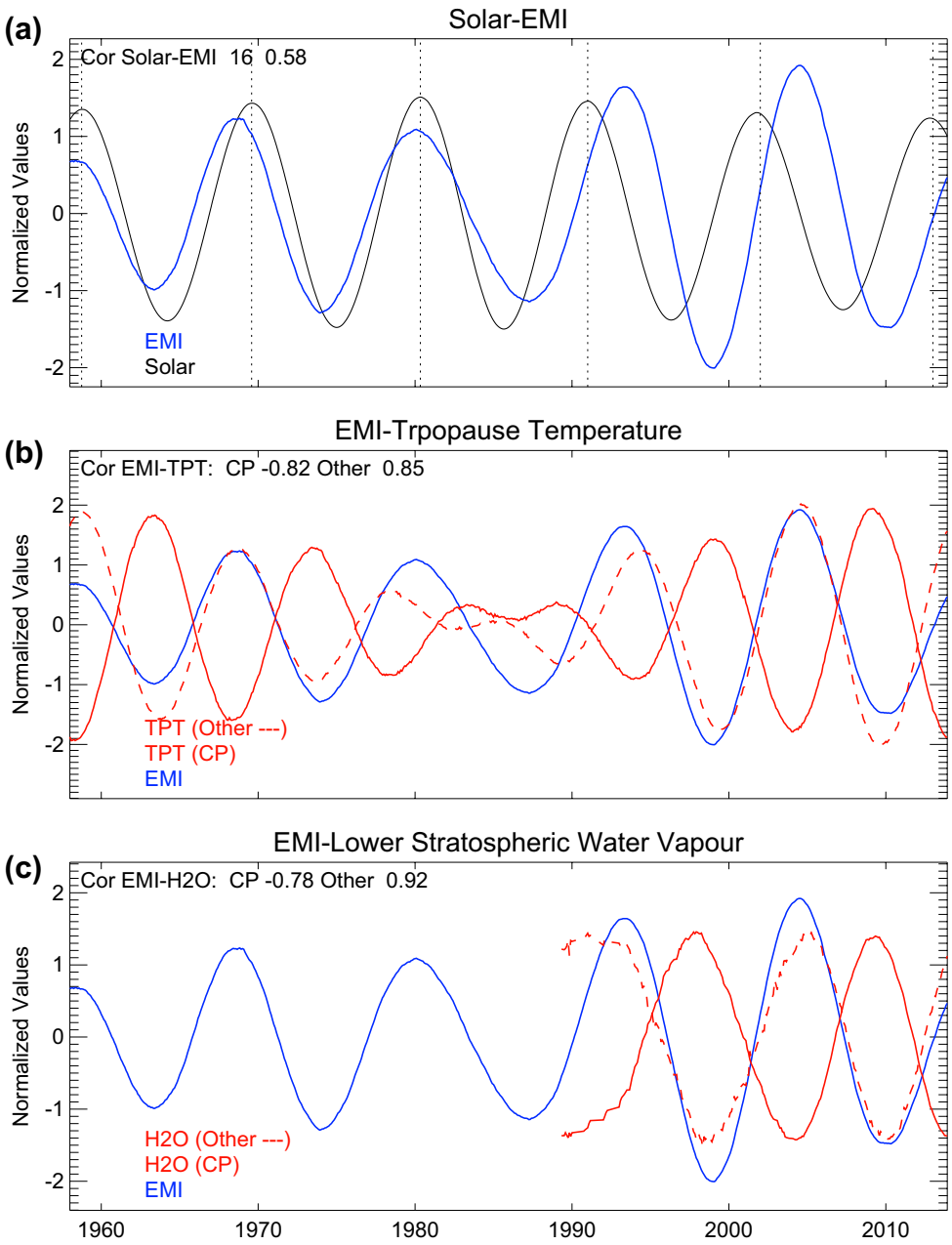

Fig. 9 The relationship between solar, SST and tropopause temperature and LS water vapour. **a** Band-pass filtered (9–13 year) observational F10.7 solar index (black) and EMI (blue). **b** Band-pass filtered EMI (blue) and tropopause temperature (using the JRA-55 reanalysis 1958–2013) averaged over the central Pacific (solid red line) and other longitudes (dashed red line) in the tropics. **c** Same as in **b**, but for LS water vapour (averaged from 100 to 80 hPa) using the SWOOSH data 1984–2013. Note that before 1991, there are a lot of missing values

the EMI and the solar cycle is shifting for different periods. For the first three cycles, the EMI is approximately in phase with the solar cycle. However, for the last two or three solar cycles, SST anomalies appear about 3 years after the solar maximum. This is because the decadal variability in EMI is not exactly 11 years and the strength of its decadal power varies with time (see Fig. S5a). Solar activity influences the EMI in its decadal variability as an external forcing, however, the EMI has its own internal decadal to multi-decadal variability, which is somehow irregular and makes it more difficult to detect solar signals.

Figure 9b shows the relationship between the EMI and tropopause temperatures. Two time series of tropical tropopause temperatures, one averaged over the central Pacific (20°S–20°N, 150°E–120°W, CP) and the other one averaged over all other longitude bands (other), are used here because of the zonal asymmetry in tropopause signals (Fig. 8). Tropical tropopause temperatures have a very good correlation with the EMI index, with a negative correlation of − 0.82 for the central Pacific and a positive correlation of 0.85 for other regions (Fig. 9b). This is consistent with the zonal structure of tropopause temperature anomalies as shown in Fig. 8 as well as in previous studies (Garfinkel et al. 2013b; Xie et al. 2014). A recent study indicates that the relationship between the ENSO and the tropical tropopause temperatures maybe nonlinear, especially for extreme

ENSO events (Garfinkel et al. 2018). However, perhaps it is not the case for this study since solar related SST signals are not that strong and are similar to El Niño Modoki rather than a conventional El Niño. At the same time, since tropopause temperatures dominate the LS water vapour content, the EMI shows also very good correlation with the LS water vapour in the tropics. A negative correlation of − 0.92 and a positive correlation of 0.78 can been seen between the EMI index and the LS water vapour (averaged from 100 to 80 hPa) over the central Pacific and other regions, respectively (Fig. 9c). Good correlations between timeseries of EMI, tropical tropopause temperatures and LS water vapour suggest that the solar related decadal variations in EMI may further impact the decadal variability in tropical tropopause temperatures and LS water vapour, with negative anomalies over the central Pacific and positive anomalies over other regions of the Pacific.

Results in this study indicate that the solar cycle is related to anomalous positive SSTs in the central Pacific and anomalous negative SSTs in the western and eastern Pacific, which resemble an El Niño Modoki event. Such SST anomalies are then amplified by positive feedbacks through oceanic subsurface currents and heat transport in the equatorial Pacific, which lead to the development of an El Niño Modoki-like signal which peaks at about 2 years after the solar maximum. Solar-induced SST signals in turn modify atmospheric circulation and convection, which gives a positive feedback to solar signals in the ocean and leads to lagged solar signals in tropical tropopause heights, tropopause temperatures and LS water vapour with a clear zonally asymmetric structure.

4 Summary and discussion

Solar signals in SSTs, the ocean and tropopause temperatures are investigated using a combination of both observations and oceanic and atmospheric reanalyses data from 1958 through 2013. Consistent with previous studies (Gray et al. 2010; Mitchell et al. 2015; Kodera et al. 2016), the solar cycle is related to enhanced temperatures and an enhanced subtropical jet in the upper stratosphere, which propagate down to the troposphere due to wave-mean flow interactions and resembles the NAM in the lower stratosphere (Matthes et al. 2006; Kodera et al. 2016). In particular, solar associated westerly anomalies in the high-latitude appear to propagate down to the troposphere preferentially in the Pacific sector and the specific mechanism for this preferential propagation is left for future work, though it may be due to the enhanced local waveguide (Figs. 1 and 2). Such westerly zonal anomalies potentially lead to anticyclonic circulation anomalies in the western and anomalous cyclonic circulations in the eastern part of Northern Pacific and a burst of anomalous westerlies in the equatorial Pacific (Fig. 3). The mid-latitude and tropical wind anomalies lead to SST anomalies, such as positive SST anomalies in the equatorial central Pacific and in the surroundings of the western coast of North America as well as negative anomalies in the equatorial western and eastern Pacific (Fig. 4), which resembles an El Niño Modoki mode.

The El Niño Modoki-like SST response persists and develops due to the Bjerknes feedback: positive SST anomalies (central Pacific) and subsequent SST gradient changes across the western Pacific lead to wind and ocean current changes near the surface (Figs. 4 and 5), which modulate the Walker circulation in the atmosphere (Figs. 4 and 7) as well as the oceanic circulation in the subsurface of the tropical Pacific (Figs. 5 and 6). Such changes in the Walker circulation and oceanic currents in turn provide positive feedbacks to the anomalous positive SSTs in the central Pacific and negative SST anomalies in the equatorial western Pacific. All these solar-induced signals in the atmosphere and the ocean peak at about 2 years after the solar maximum and decay afterwards.

So far, most solar influence studies are limited to the analysis of SSTs. Responses in the ocean have been investigated mostly in model simulations. Here, we give the first analysis of solar signals in the subsurface of the ocean with the recently available ORAS4 reanalyses. Anomalous positive ocean temperatures occur from the surface to 150 m depth in the central Pacific (Fig. 5). Further analyses of the heat transport (Fig. 6) shows a consistent (positive feedback) mechanism as proposed from the solar signals in SSTs and near surface winds.

Variations in the ocean in turn influence the overlying atmosphere. Positive SST anomalies result in more frequent deep convection and enhanced vertical motion over the central Pacific whereas negative SST anomalies in the western and eastern Pacific cause less frequent deep convection and weaker vertical motion (Fig. 7). This then results in a higher and colder tropopause over the central Pacific and a lower and warmer tropopause over the western and eastern Pacific (Figs. 7, 8). Tropopause temperature variations in turn dominate the water vapour variations in the LS over the corresponding regions (Fig. 9). As an effective greenhouse gas, feedbacks of the lower stratospheric water vapour to surface climate, e.g., the role of the LS water vapour (particularly its zonally asymmetric anomalies) in modulating the decadal variability of SSTs, await further investigation.

Previous studies have indeed reported positive anomalies in zonal mean temperatures in the LS during years with stronger solar activities. This study extends previous work by: (1) looking at the zonally asymmetric structure, and (2) investigating the solar signals in tropopause temperatures with different time lags. The tropopause temperature anomalies are consistent with the evolution of SST anomalies, which are lagged to the solar cycle with

about 1–3 years. While the atmosphere has no or very short memory, such a 2-year lag in solar related tropopause signals therefore indicates that solar variability affects the tropopause by modulating SSTs. In addition, spatial patterns of tropopause temperature and lower stratosperic water vapour are expected to be important for surface climate (Garfinkel et al. 2013a; Fu 2013; Hu et al. 2016; Wang et al. 2016).

Solar signals, from the stratosphere to the troposphere, from the mid-latitudes to the tropics, from the atmosphere to the ocean and from the ocean back to the troposphere and the tropopause region are analyzed in this study. However, there are still some caveats in our results. For example, the origin of the SST anomalies associated with the solar cycle can not be fully explained by observations only. Although we related the SST anomalies to the downward propagation of solar induced westerly anomalies from the stratosphere to the troposphere and subsequent circulation changes near the surface, there are still large uncertainties and a comprehensive mechanism awaits further research. In addition, the ocean has its own decadal variability (e.g., the El Niño Modoki and the PDO), and hence the possibility that signals in the tropical Pacific are intrinsic decadal variability unrelated to the solar cycle can not be rejected. Our study suggests, that there is some modulation of these internal variability modes by the solar cycle similar to what has been seen in the Atlantic (Thiéblemont et al. 2015). Several modeling studies have shown similar SST responses, with positive SST anomalies over the central Pacific which are lagged to the solar maximum of about 2 years (Meehl and Arblaster 2009; Misios et al. 2016). Our own previous modeling study also indicates that, without the solar cycle, the decadal variability in both SSTs and tropopause temperatures are reduced significantly (Wang et al. 2016). However, it is still challenging to simulate the correct phase of ENSO or El Niño Modoki events in a climate model. Therefore it is very difficult to simulate the correct solar signals in the Pacific using fully-coupled climate models. Our observational results await further confirmation with more modeling studies.

Acknowledgements This work was supported jointly by the National Natural Science Foundation of China (41705023, 41630421), the Postdoctoral Science Foundation of China (2017M610319), the Natural Science Foundation of Jiangsu Province (BK20170665) and the Helmholtz Centre for Ocean Research Kiel (GEOMAR, within the Helmholtz-University Young Investigators Group NATHAN). We thank the NOAA's Space Weather Prediction Center for the solar f10.7 data, the Hadley Centre for the HadISST data, the European Centre for Medium-Range Weather Forecasts for the ORAS4 data, the NOAA Chemical Sciences Division (CSD) for the SWOOSH data and the Japan Meteorological Agency for the dissemination of the JRA-55 data. We thank Jiankai Zhang, Fei Xie and Wenjuan Huo for useful discussions about the atmospheric and oceanic dynamics. We greatly appreciate Prof. Dr. Jianping Li and three anonymous reviewers for their constructive comments and suggestions.

References

Alexander MA, Vimont DJ, Chang P, Scott JD (2010) The impact of extratropical atmospheric variability on ENSO: testing the seasonal footprinting mechanism using coupled model experiments. J Clim 23(11):2885–2901

Ashok K, Behera SK, Rao SA, Weng H, Yamagata T (2007) El niño modoki and its possible teleconnection. J Geophys Res 112(C11):C11007

Baldwin MP, Dunkerton TJ (2005) The solar cycle and stratospheretroposphere dynamical coupling. J Atmos Sol Terr Phys 67(1):71–82

Balmaseda MA, Mogensen K, Weaver AT (2013) Evaluation of the ecmwf ocean reanalysis system oras4. Q J R Meteorol Soc 139(674):1132–1161

Bjerknes J (1969) Atmospheric teleconnections from the equatorial pacific. Mon Weather Rev 97(3):163–172

Chen S, Yu B, Chen W (2014) An analysis on the physical process of the influence of AO on ENSO. Clim Dyn 42(3–4):973–989

Chiodo G, Marsh DR, Garcia-Herrera R, Calvo N, García JA (2014) On the detection of the solar signal in the tropical stratosphere. Atmos Chem Phys 14(11):5251–5269

Davis SM, Rosenlof KH, Hassler B, Hurst DF, Read WG, Vömel H, Selkirk H, Fujiwara M, Damadeo R (2016) The stratospheric water and ozone satellite homogenized (swoosh) database: a long-term database for climate studies. Earth Syst Sci Data 8(2):461–490

Deser C, Alexander MA, Xie S-P, Phillips AS (2010) Sea surface temperature variability: patterns and mechanisms. Annu Rev Mar Sci 2(1):115–143

Dessler A, Schoeberl M, Wang T, Davis S, Rosenlof K, Vernier J-P (2014) Variations of stratospheric water vapor over the past three decades. J Geophys Res 119(22):12–588

Dessler a E, Schoeberl MR, Wang T, Davis SM, Rosenlof KH (2013) Stratospheric water vapor feedback. Proc Natl Acad Sci USA 110(45):18087–91

DiNezio PN, Clement AC, Vecchi GA, Soden BJ, Kirtman BP, Lee S-K (2009) Climate response of the equatorial pacific to global warming. J Clim 22(18):4873–4892

Ding Q, Fu Q (2017) A warming tropical central Pacific dries the lower stratosphere. Clim Dyn 0(0):1–15

Fu Q (2013) Ocean–atmosphere interactions: bottom up in the tropics. Nat Clim Change 3(11):957–958

Fueglistaler S, Liu Y, Flannaghan T, Haynes P, Dee D, Read W, Remsberg E, Thomason L, Hurst D, Lanzante J et al (2013) The relation between atmospheric humidity and temperature trends for stratospheric water. J Geophys Res 118(2):1052–1074

Garfinkel C, Waugh D, Oman L, Wang L, Hurwitz M (2013a) Temperature trends in the tropical upper troposphere and lower stratosphere: connections with sea surface temperatures and implications for water vapor and ozone. J Geophys Res 118(17):9658–9672

Garfinkel CI (2017) Might stratospheric variability lead to improved predictability of ENSO events? Environ Res Lett 12(3):2018–2020

Garfinkel CI, Gordon A, Oman LD, Li F, Davis S, Pawson S (2018) Nonlinear response of tropical lower-stratospheric temperature and water vapor to ENSO. Atmos Chem Phys 18(7):4597–4615

Garfinkel CI, Hurwitz MM, Oman LD, Waugh DW (2013b) Contrasting effects of central pacific and eastern pacific el nio on stratospheric water vapor. Geophys Res Lett 40(15):4115–4120

Gettelman A et al (2010) Multimodel assessment of the upper troposphere and lower stratosphere: Tropics and global trends. J Geophys Res 115:D00M08. https://doi.org/10.1029/2009JD013638

Gilford DM, Solomon S, Portmann RW (2016) Radiative impacts of the 2011 abrupt drops in water vapor and ozone in the tropical tropopause layer. J Clim 29(2):595–612

Gray LJ, Beer J, Geller M, Haigh JD, Lockwood M, Matthes K, Cubasch U, Fleitmann D, Harrison G, Hood L, Luterbacher J, Meehl GA, Shindell D, van Geel B, White W (2010) Solar influences on climate. Rev Geophys 48(4):RG4001

Gray LJ, Scaife AA, Mitchell DM, Osprey S, Ineson S, Hardiman S, Butchart N, Knight J, Sutton R, Kodera K (2013) A lagged response to the 11 year solar cycle in observed winter atlantic/european weather patterns. J Geophys Res 118(24):13–405

Harada Y, Kamahori H, Kobayashi C, Endo H, Kobayashi S, Ota Y, Onoda H, Onogi K, Miyaoka K, Takahashi K (2016) The jra-55 reanalysis: representation of atmospheric circulation and climate variability. J Meteorol Soc Jpn Ser II 94(3):269–302

Hegglin M, Plummer D, Shepherd T, Scinocca J, Anderson J, Froidevaux L, Funke B, Hurst D, Rozanov A, Urban J et al (2014) Vertical structure of stratospheric water vapour trends derived from merged satellite data. Nat Geosci 7(10):768–776

Hoskins BJ, Ambrizzi T (1993) Rossby wave propagation on a realistic longitudinally varying flow. J Atmos Sci 50:1661–1671

Hu D, Tian W, Guan Z, Guo Y, Dhomse S (2016) Longitudinal asymmetric trends of tropical cold-point tropopause temperature and their link to strengthened walker circulation. J Clim 29(21):7755–7771

Hu D, Tian W, Xie F, Shu J, Dhomse S (2014) Effects of meridional sea surface temperature changes on stratospheric temperature and circulation. Adv Atmos Sci 31(4):888–900

Huo W, Xiao Z (2017) Modulations of solar activity on el niño modoki and possible mechanisms. J Atmos Sol Terr Phys 160:34–47

Hurst DF, Oltmans SJ, Vömel H, Rosenlof KH, Davis SM, Ray EA, Hall EG, Jordan AF (2011) Stratospheric water vapor trends over boulder, colorado: analysis of the 30 year boulder record. J Geophys Res 116(D2):D02306

Ingleby B, Huddleston M (2007) Quality control of ocean temperature and salinity profiles historical and real-time data. J Mar Syst 65(1–4):158–175

Kobayashi S, Ota Y, Harada Y, Ebita A, MORIYA M, ONODA H, ONOGI K, KAMAHORI H, KOBAYASHI C, ENDO H, MIYAOKA K, TAKAHASHI K (2015) The jra-55 reanalysis: general specifications and basic characteristics. J Meteorol Soc Jpn Ser II 93(1):5–48

Kodera K, Kuroda Y (2002) Dynamical response to the solar cycle. J Geophys Res 107(D24):ACL5-1–ACL5-12

Kodera K, Thiéblemont R, Yukimoto S, Matthes K (2016) How can we understand the solar cycle signal on the earths surface? Atmos Chem Phys Discuss 138:1–33

Kopp G, Lean JL (2011) A new, lower value of total solar irradiance: evidence and climate significance. Geophys Res Lett 38(1):L01706

Lean JL, White OR, Skumanich A (1995) On the solar ultraviolet spectral irradiance during the maunder minimum. Global Biogeochem Cycles 9(2):171–182

Marsh DR, Garcia RR (2007) Attribution of decadal variability in lower-stratospheric tropical ozone. Geophys Res Lett 34(21):21807

Matthes K, Kuroda Y, Kodera K, Langematz U (2006) Transfer of the solar signal from the stratosphere to the troposphere: Northern winter. J Geophys Res Atmos 111(D6):D06108

Meehl GA, Arblaster JM (2009) A lagged warm event-like response to peaks in solar forcing in the pacific region. J Clim 22(13):3647–3660

Meehl GA, Arblaster JM, Matthes K, Sassi F, van Loon H (2009) Amplifying the pacific climate system response to a small 11-year solar cycle forcing. Science 325(5944):1114–1118

Misios S, Mitchell DM, Gray LJ, Tourpali K, Matthes K, Hood L, Schmidt H, Chiodo G, Thiblemont R, Rozanov E, Krivolutsky A (2016) Solar signals in cmip-5 simulations: effects of atmosphereocean coupling. Q J R Meteorol Soc 142(695):928–941

Misios S, Schmidt H (2012) Mechanisms Involved in the amplification of the 11-yr solar cycle signal in the tropical pacific ocean. J Clim 25(14):5102–5118

Mitchell DM, Gray LJ, Fujiwara M, Hibino T, Anstey JA, Ebisuzaki W, Harada Y, Long C, Misios S, Stott PA, Tan D (2014) Signatures of naturally induced variability in the atmosphere using multiple reanalysis datasets. Q J R Meteorol Soc 141(691):2011–2031

Mitchell DM, Misios S, Gray LJ, Tourpali K, Matthes K, Hood L, Schmidt H, Chiodo G, Thiblemont R, Rozanov E, Shindell D, Krivolutsky A (2015) Solar signals in cmip-5 simulations: the stratospheric pathway. Q J R Meteorol Soc 141(691):2390–2403

Mogensen K, Alonso Balmaseda M, Weaver A (2012) The NEMOVAR ocean data assimilation system as implemented in the ECMWF ocean analysis for System 4. Tech Memo 668(February):1–59

Nakamura T, Tachibana Y, Shimoda H (2007) Importance of cold and dry surges in substantiating the NAM and ENSO relationship. Geophys Res Lett 34(22):4–7

Randel WJ, Wu F, Vömel H, Nedoluha GE, Forster P (2006) Decreases in stratospheric water vapor after 2001: links to changes in the tropical tropopause and the brewer-dobson circulation. J Geophys Res 111(D12):D12312

Randel WJ, Garcia RR, Calvo N, Marsh D (2009) Enso influence on zonal mean temperature and ozone in the tropical lower stratosphere. Geophys Res Lett 36:L15822. https://doi.org/10.1029/2009GL039343

Rayner N, Parker D, Horton E, Folland C, Alexander L, Rowell D, Kent E, Kaplan A (2003) Global analyses of sea surface temperature, sea ice, and night marine air temperature since the late nineteenth century. J Geophys Res 108(D14):4407–4453

Rosenlof KH, Reid GC (2008) Trends in the temperature and water vapor content of the tropical lower stratosphere: Sea surface connection. J Geophys Res 113(D6):D06107

Roy I, Haigh JD (2010) Solar cycle signals in sea level pressure and sea surface temperature. Atmos Chem Phys 10(6):3147–3153

Scaife AA, Ineson S, Knight JR, Gray L, Kodera K, Smith DM (2013) A mechanism for lagged north atlantic climate response to solar variability. Geophys Res Lett 40(2):434–439

Schieferdecker T, Lossow S, Stiller G, von Clarmann T (2015) Is there a solar signal in lower stratospheric water vapour? Atmos Chem Phys 15(17):9851–9863

Solomon S, Rosenlof KH, Portmann RW, Daniel JS, Davis SM, Sanford TJ, Plattner G-K (2010) Contributions of stratospheric water vapor to decadal changes in the rate of global warming. Science 327(5970):1219–1223

Thiéblemont R, Matthes K, Omrani N-E, Kodera K, Hansen F (2015) Solar forcing synchronizes decadal north atlantic climate variability. Nat Commun 6:8268

Thompson DW, Wallace JM (2000) Annular modes in the extratropical circulation. part i: Month-to-month variability. J Clim 13(5):1000–1016

Thompson DWJ, Kennedy JJ, Wallace JM, Jones PD (2008) A large discontinuity in the mid-twentieth century in observed global-mean surface temperature. Nature 453(7195):646–649

Torrence C, Compo GP (1998) A practical guide to wavelet analysis. Bull Am Meteorol Soc 79(1):61–78

Tung K-K, Zhou J (2010) The pacific's response to surface heating in 130 yr of sst: La niña-like or el niño-like? J Atmos Sci 67(8):2649–2657

van Loon H, Meehl GA (2008) The response in the pacific to the sun's decadal peaks and contrasts to cold events in the southern oscillation. J Atmos Sol Terr Phys 70(7):1046–1055

Vimont DJ, Battisti DS, Hirst AC (2001) Footprinting: a seasonal connection between the tropics and mid-latitudes. Geophys Res Lett 28(20):3923–3926

Wang JS, Seidel DJ, Free M (2012) How well do we know recent climate trends at the tropical tropopause? J Geophys Res 117(D16):09118

Wang W, Matthes K, Omrani N-E, Latif M (2016) Decadal variability of tropical tropopause temperature and its relationship to the pacific decadal oscillation. Sci Rep 6:29537

Wang W, Matthes K, Schmidt T (2015) Quantifying contributions to the recent temperature variability in the tropical tropopause layer. Atmos Chem Phys 15(10):5815–5826

Wang W, Matthes K, Schmidt T, Neef L (2013) Recent variability of the tropical tropopause inversion layer. Geophys Res Lett 40(23):6308–6313

Wang Y, Su H, Jiang JH, Livesey NJ, Santee ML, Froidevaux L, Read WG, Anderson J (2017) The linkage between stratospheric water vapor and surface temperature in an observation-constrained coupled general circulation model. Clim Dyn 48(7–8):2671–2683

White WB, Lean J, Cayan DR, Dettinger MD (1997) Response of global upper ocean temperature to changing solar irradiance. J Geophys Res 102(C2):3255–3266

White WB, Liu Z (2008) Resonant excitation of the quasi-decadal oscillation by the 11-year signal in the sun's irradiance. J Geophys Res 113(C1):C01002

Wigley T (2006) Appendix a: Statistical issues regarding trends, in temperature trends in the lower atmosphere: steps for understanding and reconciling differences. In: Karl TR, Hassol SJ, Miller CD, Murray WL (eds) A report by climate change science program and the subcommittee on global change research, Washington, DC, USA. UNT Digital Library, pp 129–139

Xie F, Li J, Tian W, Feng J, Huo Y (2012) Signals of el niño modoki in the tropical tropopause layer and stratosphere. Atmos. Chem Phys 12(11):5259–5273

Xie F, Li J, Tian W, Fu Q, Jin FF, Hu Y, Zhang J, Wang W, Sun C, Feng J, Yang Y, Ding R (2016) A connection from Arctic stratospheric ozone to El Nino-Southern oscillation. Environ Res Lett 11(12):1–12

Xie F, Li J, Tian W, Li Y, Feng J (2014) Indo-pacific warm pool area expansion, modoki activity, and tropical cold-point tropopause temperature variations. Sci Rep 4:4552

Yeh S-W, Kug J-S, Dewitte B, Kwon M-H, Kirtman BP, Jin F-F (2009) El Niño in a changing climate. Nature 461(7263):511–514

Zhou J, Tung K-K (2010) Solar cycles in 150 years of global sea surface temperature data. J Clim 23(12):3234–3248